Lattice Kinetic Scheme for Generalised Coordinates and Curved Spaces

M. Mendoza

ETH Zürich, Computational Physics for Engineering Materials, Institute for Building Materials, Wolfgang-Pauli-Str. 27, HIT, CH-8093 Zürich, Switzerland.

mmendoza@ethz.ch

S. Succi

Istituto per le Applicazioni del Calcolo C.N.R., Via dei Taurini, 19 00185, Rome Italy, and Freiburg Institute for Advanced Studies, Albertstrasse, 19, D-79104, Freiburg, Germany.

succi@iac.cnr.it

H. J. Herrmann

ETH Zürich, Computational Physics for Engineering Materials, Institute for Building Materials, Schafmattstrasse 6, HIF, CH-8093 Zürich, Switzerland.

hjherrmann@ethz.ch

We present a new lattice kinetic method to simulate fluid dynamics in curvilinear geometries and curved spaces. A suitable discrete Boltzmann equation is solved in contravariant coordinates, and the equilibrium distribution function is obtained by a Hermite polynomials expansion of the Maxwell-Boltzmann distribution, expressed in terms of the contravariant coordinates and the metric tensor. To validate the model, we calculate the critical Reynolds number for the onset of the Taylor-Couette instability between two concentric cylinders, obtaining excellent agreement with the theory. In order to extend this study to more general geometries, we also calculate the critical Reynolds number for the case of two concentric spheres, finding good agreement with experimental data, and the case of two concentric tori, where we have found that it is around 10% larger than the respective values for the two concentric cylinders.

Keywords: curved spaces, curvilinear coordinates, lattice Boltzmann

1. Introduction

Many situations of physical interest imply fluids moving in curved spaces, such as atmospheric flow[1], flows in curved soap films[2], plasma flow in the solar photosphere[3], and plasma fusion[4], among others. However, up to now, the study of such systems has been limited to relatively simple geometries, because once the curved space becomes more complicated, the use of one common underlying coordinate system (e.g. cartesian, spherical, or cylindrical) leads to an expensive use of computational resources and a poor approximation of the spatial curvature and the boundary conditions.

One consequence of the motion of fluids in curved spaces are centrifugal instabilities, like Taylor-Couette, which have been extensively studied for the case of two concentric rotating cylinders[5,6], and also for the case of two concentric rotating spheres[7]. However, the exploration of these instabilities in more general geometries has been limited by the fact that it is not easy to implement an efficient numerical method allowing for arbitrary curvatures.

In the last decade, the use of lattice Boltzmann (LB) methods to solve the minimal Boltzmann kinetic equation, rather than discretising and solving directly the equations of continuum fluid mechanics, has attracted considerable interest as an alternative to simulate fluid dynamics[8,9], including relativistic flows[10,11,12], due to its efficiency and accuracy. However, to date, the overwhelming majority of LB applications are directed towards classical fluids in Cartesian coordinates, using cubic cells to discretise the spatial and velocity coordinates, thereby limiting the use of LB models to fluid dynamics in flat spaces.

Recently, a number of approaches to adapt the lattice Boltzmann method to general geometries have been developed. Halliday et al.[13] and Niu et al.[14] adapted the LB model to cylindrical coordinates, and Klales et. al.[15] proposed a model in two dimensions introducing an adaptive geometry, which consists in changing the discretisation in time. However, a three-dimensional LB equation capable of handling fluids in arbitrary geometries, has not been achieved yet. The study of fluids in very complicated geometries, where non-inertial forces play a major role, and where due to the symmetry of the system the choice of an appropriate coordinate system, may significantly facilitate the formulation and implementation of the boundary conditions, poses in general a formidable task.

In this paper, we develop a lattice Boltzmann model to simulate fluid dynamics in general geometries, and, additionally, we calculate the critical Reynolds number for the onset of the Taylor-Couette instability in the case of two concentric rotating tori.

2. Model Description

In order to adapt the LB scheme to general geometries, the metric tensor g_{ij} and the Christoffel symbol Γ^i_{kj} need to be included in the model. The former characterises the way to measure distances in space, while the latter is responsible for the non-inertial forces. The corresponding hydrodynamic equations are obtained by replacing the partial derivatives by covariant ones, in both the mass continuity and the momentum conservation equations. After some algebraic manipulations, the hydrodynamic equations read as follows:

$$\partial_t \rho + (\rho u^i)_{;i} = 0 \quad , \quad \partial_t(\rho u^i) + T^{ij}_{;j} = 0 \quad , \tag{1}$$

where the notation $_{;i}$ denotes the covariant derivative with respect to spatial component i. The energy tensor T^{ij} is given by, $T^{ij} = P g^{ij} + \rho u^i u^j - \mu(g^{lj} u^i_{;l} + g^{il} u^j_{;l} + g^{ij} u^l_{;l})$, where P is the hydrostatic pressure, u^i the i-th contravariant component of

the velocity, g^{ij} the contravariant metric tensor, ρ is the density of the fluid, and μ is the dynamic shear viscosity.

Since lattice Boltzmann methods are based on kinetic theory, we start our model construction by writing the Maxwell-Boltzmann distribution and the Boltzmann equation in general geometries. The former takes the form[16]:

$$f^{\rm eq} = \frac{\sqrt{g}\rho}{(2\pi\theta)^{3/2}} \exp\left[-\frac{1}{2\theta} g_{ij}(\xi^i - u^i)(\xi^j - u^j)\right] \quad , \tag{2}$$

where g is the determinant of the metric g_{ij}, and θ is the normalized temperature. The macroscopic and microscopic velocities, u^i and ξ^i are both normalised with the speed of sound $c_s = \sqrt{k_B T_0/m}$, k_B being the Boltzmann constant, T_0 the typical temperature, and m the mass of the particles. Note that the metric tensor appears explicitly in the distribution function, due to the fact that the kinetic energy is a quadratic function of the velocity, which in a manifold, writes as, $u^i u_i = g_{ij} u^i u^j$. To recover the macroscopic fluid dynamic equations, we have to extract the moments from the equilibrium distribution function. The four first moments of the Maxwellian distribution function on a manifold are given by,

$$\rho = \int f d\xi \quad , \quad \rho u^i = \int f \xi^i d\xi \quad , \tag{3a}$$

$$\rho\theta g^{ij} + \rho u^i u^j = \int f \xi^i \xi^j d\xi \quad , \tag{3b}$$

$$\rho\theta(u^i g^{jk} + u^j g^{ik} + u^k g^{ij}) + \rho u^i u^j u^k = \int f \xi^i \xi^j \xi^k d\xi. \tag{3c}$$

These moments are sufficient to reproduce the mass and the momentum conservation equations. Here, for simplicity we have used $d\xi$ to denote $d\xi^1 d\xi^2 d\xi^3$ and the Jacobian of the integration is already included in the Maxwell Boltzmann distribution, through the term $\sqrt{g}$.

In the absence of external forces, in the standard theory of the Boltzmann equation, the single particle distribution function $f(x^i, \xi^i, t)$ evolves, according to the equation, $\partial_t f + \xi^i \partial_i f = \mathcal{C}(f)$, where $\mathcal{C}$ is the collision term, which, using the BGK approximation, can be written as, $\mathcal{C} = -(1/\tau)(f - f^{\rm eq})$, with the single relaxation time τ. This equation can be obtained from a more general expression, $df/dt = \mathcal{C}(f)$, where the total time derivative now includes a streaming term in velocity space due to external forces, $\frac{df}{dt} = \partial_t f + \frac{dx^i}{dt}\partial_i f + \frac{dp^i}{dt}\partial_{p^i} f$, with p^i the i-th contravariant component of the momentum of the particles. Using the definition of velocity, $\xi^i = dx^i/dt$, and due to the fact that the particles move along geodesics, which implies the equation of motion $dp^i/dt = -\Gamma^i_{kl} p^k p^l$, we can write the Boltzmann equation as,

$$\partial_t f + \xi^i \partial_i f - \Gamma^i_{jk} \xi^j \xi^k \partial_{\xi^i} f = \mathcal{C}(f) \quad , \tag{4}$$

where we have used the definition of the momentum, $p^i = m\xi^i$. Note that the third term of the lhs carries all the information on inertial forces. Thus, all the ingredients

required to model a fluid in general geometries within the Boltzmann equation are now in place.

In order to formulate a corresponding lattice Boltzmann model, we implement an expansion of the Maxwell-Boltzmann distribution in Hermite polynomials, so as to recover the moments of the distribution function up to third order in velocities, as it is needed to correctly reproduce hydrodynamic behaviour. The expansion of the Maxwell-Boltzmann distribution was introduced by Grad in his 13 moment system[17]. Since this expansion is performed in velocity space, and the metric only depends on the spatial coordinates, we expect such an expansion to preserve its validity also in the case of a general manifold. We have followed a similar procedure as the one described in Refs. [18,19].

For the discretization of the Maxwell Boltzmann distribution (2) and the Boltzmann equation (4), we need a cell configuration that supports the expansion up to third order in Hermite polynomials. Our model construction was tested with the discrete configurations $D3Q19$ and $D3Q27$, with no success, due to the fact that such cell configurations do not provide the necessary symmetry to reproduce Eq. (3c). However, the $D3Q41$ configuration proposed by Chikatamarla and Karlin[20], corresponds to the minimum configuration in three dimensions that supports third order isotropy, as well as a H-theorem for future entropic extensions [21,22] of the present work.

In the following, we shall use the notation c^i_λ to denote the vector number λ and the contravariant component i. Thus, the discrete Boltzmann equation for our model takes the form, $f_\lambda(x^i + c^i_\lambda \delta t, t + \delta t) - f_\lambda(x^i, t) = -\frac{\delta t}{\tau}(f_\lambda - f^{\rm eq}_\lambda) + \delta t \mathcal{F}_\lambda$, where $\mathcal{F}_\lambda$ is the forcing term, which contains the Christoffel symbols, and $f^{\rm eq}_\lambda$ is the discrete form of the Maxwell-Boltzmann distribution, Eq. (2). The relevant physical information about the fluid and the geometry of the system is contained in these two terms that are explicitly written in Ref.[23].

Note, that since the contravariant components of the velocity are free from space-dependent metric factors, they lend themselves to the standard lattice Boltzmann discretisation of velocity space. All the metric and inertial information is conveyed into the generalised local equilibria and forcing term, respectively. These features are key to the LB formulation in general coordinates.

The macroscopic variables are obtained with the relations, $\rho = \sum_{\lambda=0}^{41} f_\lambda$, $\rho u^i = \sum_{\lambda=0}^{41} f_\lambda c^i_\lambda$.

In order to recover the correct macroscopic fluid equations, via a Chapman-Enskog expansion, the other moments, Eq. (3), also need to be reproduced. A straightforward calculation shows that the equilibrium distribution function $f^{\rm eq}_\lambda$ meets the requirement. The shear viscosity of the fluid also can be calculated as $\mu = \rho(\tau - 1/2)c_s^2 \delta t$. In this way one can calculate the fluid motion in spaces having arbitrary local curvatures.

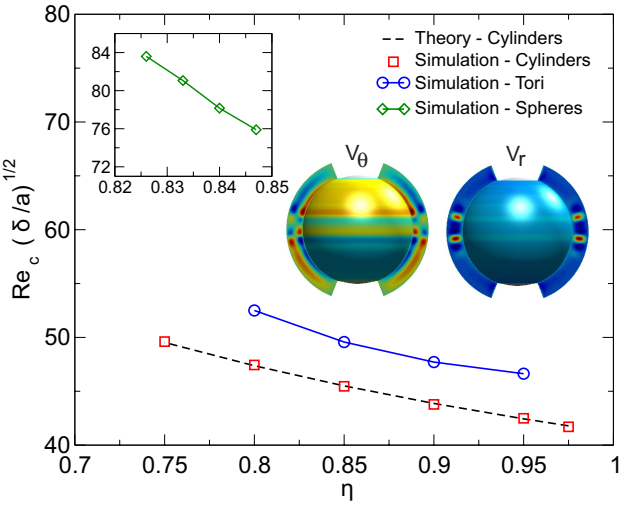

Fig. 1. Critical Reynolds number Re_c, as a function of the parameter $\eta = a/b$ for the onset of the Taylor-Couette instability for two concentric rotating cylinders (red) and tori (blue). Numerical values for the case of the cylinders agree with theoretical values. The left inset shows the critical Reynolds number for the case of two concentric spheres, and the two coloured spheres the radial and axial components of the fluid velocity for the spherical case. Blue and red colours denote low and high values, respectively.

3. Validation and Results

To provide numerical validation of our model we study the Taylor-Couette instability, which develops between two concentric rotating cylinders. We calculate the critical Reynolds number, Re_c, which characterises the transition between stable Couette flow and Taylor vortex flow. To this purpose, we use the metric tensor for cylindrical coordinates (r, θ, z), $g_{rr} = 1$, $g_{\theta\theta} = r^2$, and $g_{zz} = 1$, where r is the radial coordinate, θ is the azimuthal angle, and z the axial coordinate. Thus, the non-vanishing Christoffel symbols for this metric are given by $\Gamma^r_{\theta\theta} = -r$, and $\Gamma^\theta_{r\theta} = \Gamma^\theta_{\theta r} = 1/r$.

In our system, the inner cylinder has radius a and the outer one radius b. We performed several simulations, by varying the Reynolds number for different aspect ratios $\eta = a/b$. The Reynolds number, assuming that the outer cylinder is fixed, can be defined as $Re = (a\delta/\nu)d\theta/dt$ where $d\theta/dt$ is the angular speed of the inner cylinder and $\delta = b - a$. The inner radius a is always set to $a = 1$, and for a given value of η, the outer radius b and δ are calculated. In order to vary Re, at fixed η, we change the angular velocity of the inner cylinder. For this simulation, we use a rectangular lattice of $128 \times 1 \times 256$ cells and choose $\tau = 1$ (all values are written in numerical units). We use periodic boundary conditions in the θ and z coordinates and fixed boundary conditions in the r coordinate. We simulate 10^5 times steps in 176 minutes, using one core on an Intel(R) Core(TM) 2 Quad CPU Q9650 at 3.00GHz.

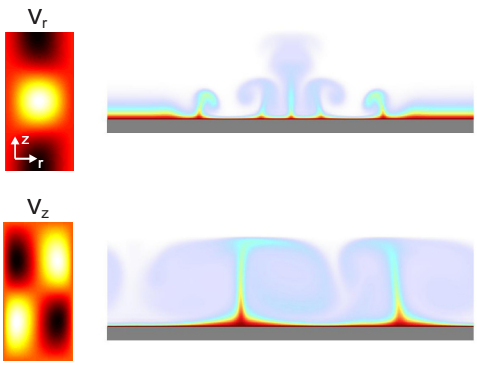

Fig. 2. Taylor-Couette flow instability for the case of two rotating cylinders. Here, we observe the vortices (bottom-right) as a consequence of inertial forces, and a snapshot of a state at the onset of the instability (top-right). The colors denote the magnitude of the fluid velocity. In addition, at the left we see the radial (top) and axial (bottom) components of the fluid velocity, where yellow and dark colours denote high and low values, respectively.

In Fig. 1, we report the critical Reynolds number as a function of η, as predicted by the simulation and compared with the theoretical values from Ref. [24], finding excellent agreement. On the left in Fig. 2, we observe the radial and axial components of the velocity. Note that, as expected from the theory, the axial wave length of the convection rolls is twice the distance between the cylinders, δ. To model the Taylor-Couette vortices at higher Reynolds numbers, we use a lattice of $128\times1\times512$ cells, and we set $d\theta/dt = 1$, $\delta = 0.128$, $a = 1$, and $b = 1.128$, obtaining a Reynolds number of $Re \sim 700$. Fig. 2 illustrates the vortices associated with this configuration. Note that at this Reynolds number, the vortices start to become asymmetric and, upon waiting sufficiently long, the system becomes unstable.

For the case of two rotating spheres, we consider the inner sphere with radius a and the outer one with radius b. We use the coordinate system of the sphere (r, ϕ, θ), being r the radial, ϕ the azimuthal, and θ the polar coordinates. The non-vanishing components of the metric tensor are $g_{rr} = 1$, $g_{\phi\phi} = r^2 \sin^2(\theta)$, and $g_{\theta\theta} = r^2$. The Christoffel symbols can be calculated from the metric tensor by using differential geometry relations. Note that our simulation region does not include the poles because there, the determinant of the metric tensor becomes zero and therefore it is not possible to calculate its inverse. To solve this, we simulate the region $\theta \in (\pi/6, 5\pi/6)$. We set $\tau = 0.8$ and use a lattice of size $32\times1\times384$. In order to vary the Reynolds number we change the azimuthal velocity $d\phi/dt$. The boundary conditions have been chosen periodic for ϕ, and fixed for r and θ. In the inset (left) of Fig. 1, we show the critical Reynolds number for different configurations which is in good agreement with the experimental values given in Ref. [7]. In this figure, we can also observe the radial and polar components of the velocity, and see that there are two small vortices located at the equator and two big ones at high and low latitudes.

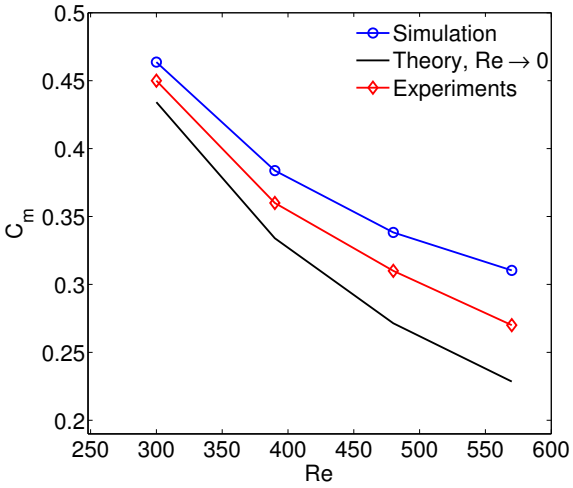

Fig. 3. Comparison of the torque coefficient as a function of the Reynolds number, for the case of two concentric rotating spheres, with theoretical and experimental data.

We have also measured the torque coefficient defined by,

$$T_r = 2\pi a^3 \int_0^{\pi} \sigma_{r\phi} \sin^2(\theta) d\theta \quad , \tag{5}$$

where $\sigma_{r\phi}$ is the shear stress tensor, which in the context of lattice kinetic theory can be calculated by,

$$\sigma^{\alpha\beta} = \left(1 - \frac{1}{2\tau}\right) \sum_{\lambda}^{41} (f_\lambda - f_\lambda^{\rm eq}) c_\lambda^\alpha c_\lambda^\beta \quad . \tag{6}$$

The torque coefficient is then computed via the following relation [25]

$$C_m = \frac{T_r}{\frac{1}{2}\rho a^5 \left(\frac{d\phi}{dt}\right)^2} \quad . \tag{7}$$

In Fig. 3, we show the comparison between our results, the theory for $Re \to 0$ and the experiments[26,25]. We find reasonable agreement with the experiments. The small discrepancy can be due to the approximation taken in Eq. (6) and the small lattice resolution used for the radial coordinate.

In order to study the Taylor-Couette instability for the case of two concentric rotating tori, which to our knowledge has never been explored before, we use a lattice of size $64 \times 128 \times 64$ cells in the orthogonal coordinate system of the torus, (r, u, v), being r the radial, u the axial, and v the tangential coordinates. The Christoffel symbols and the components of the metric tensor can be readily calculated from differential geometry relations. The major radius of the tori has been taken as 4.0 and the relaxation time $\tau = 1$, in numerical units. The other parameters are

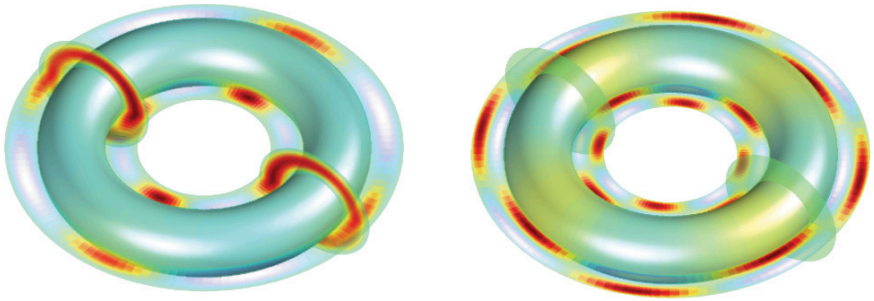

Fig. 4. Vortices generated by inertial effects for two concentric rotating tori. The radial (right) and axial (left) components of the velocity, are shown. Transparent blue and red colours code for negative and positive values, respectively. The snapshot was taken at $t = 80000$ for $Re = 205$.

the same as in the previous simulations, and to vary the Reynolds number we change the tangential velocity dv/dt. In this case, a and b are the minor radii of the inner and outer tori, respectively. We use periodic boundary conditions for the coordinates u and v, and fixed boundaries for r. Fig. 4 illustrates the vortices of the instability generated by the inertial forces, and we observe that, in analogy with the cylindrical case, there are vortices and oscillations in the axial component of the velocity (analogous to the z component of the cylinder, see Fig. 2). In addition, the critical Reynolds numbers for different configurations can be observed in Fig. 1, showing values around 10% larger than for the case of cylinders.

3.1. *Convergence Study*

To check the convergence of the model, we simulate the Poiseuille profile for the velocity on a two-dimensional ring. For this purpose, we use the metric tensor in polar coordinates, $g_{rr} = 1$, $g_{\theta\theta} = r^2$, and $g_{zz} = 1$, where r is the radial coordinate, θ is the azimuthal angle, and z the axial coordinate. Thus, the non-vanishing Christoffel symbols for this metric are given by, $\Gamma^r_{\theta\theta} = -r$, and $\Gamma^\theta_{r\theta} = \Gamma^\theta_{\theta r} = 1/r$.

Our system consists of a two-dimensional ring with inner radius a and outer one b. On this ring, we impose a constant force f_a in the θ-direction. For the simulation we choose $\tau = 0.6$. The forcing term f_a is set to 0.05. All numbers are expressed in numerical units. The inner radius of the ring is taken as $a = 1.0$ and the outer radius as $b = 1.064$. We have taken periodic boundary conditions in the direction θ and z, and free boundary conditions at $r = 1.0$ and $r = 1.064$.

To obtain a quantitative measure of the convergence we use the Richardson extrapolation method[27,28]. In this method, given any quantity $A(\delta x)$ that depends on the mesh spacing δx, we can make an estimation of order n of the exact solution

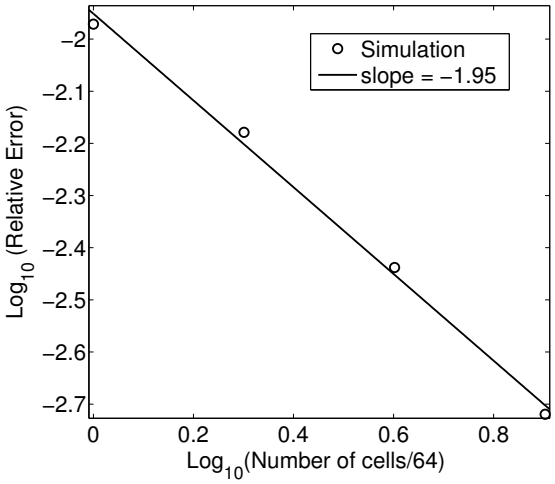

Fig. 5. Relative convergence error as a function of the number of grid points. Here, the relative error is calculated by takening the mean value of the relative errors at every location grid point.

A by using

$$A = \lim_{\delta x \to 0} A(\delta x) \approx \frac{2^n A\left(\frac{\delta x}{2}\right) - A(\delta x)}{2^n - 1} + O(\delta x^{n+1}) \quad , \tag{8}$$

with errors $O(\delta x^{n+1})$ of order $n+1$. Thus the relative error between the value $A(\delta x)$ and the "exact" solution A can be calculated by

$$E_r(\delta x) = \left| \frac{A(\delta x) - A}{A} \right| \quad . \tag{9}$$

In our case, the quantity A is the fluid density ρ, when the fluid reaches the steady state, and we set up $n = 2$. Indeed, the relative error with respect to the "exact solution" decreases rapidly with increasing grid resolution (see Fig. 5) and we can see that the present scheme exhibits a near second-order convergence. This is basically in line with the convergence properties of classical LB schemes.

Although this convergence test consists on a one-dimensional simulation, it has been implemented using a single column of three-dimensional cubic cells. Therefore, this system is equivalent to have two three-dimensional and concentric cylinders where axial and azimuthal symmetries have been imposed. As a consequence, the conclusions on this section also apply to three-dimensional cases.

4. Conclusions

Summarising, we have developed a new lattice Boltzmann model to simulate fluid dynamics in general non-cartesian geometries. The model has been validated on the Taylor-Couette instability for the case of two concentric rotating cylinders. In

our case, inner cylinder is rotating with a certain speed and the outer one is fixed, obtaining vortices and the critical Reynolds number for the onset of the instability for several configurations, in excellent agreement with the theory. In addition, we have also studied the case of the Taylor-Couette instability for the case of two concentric spheres, and found good agreement with experimental data.

To extend our study to yet unexplored more general geometries, we studied the case of the Taylor-Couette instability in two concentric rotating tori, finding that the critical Reynolds number for the onset of the instability is larger than the one for the cylinder. In principle, one could generalise this, also to more complex geometries, e.g. parabolic, Möbius band, trefoil knots, to name but a few.

By solving the Navier-Stokes equations in contravariant coordinates, which can be represented on a cubic lattice precisely in the format requested by the lattice Boltzmann formulation, the present model opens up the possibility to study fluid dynamics in smooth manifolds by retaining the outstanding simplicity and computational efficiency of the standard lattice Boltzmann method in cartesian coordinates.

References

1. Dutton, J.A., *The Ceaseless Wind: An Introduction to the Theory of Atmospheric Motion*, Phoenix Edition Series, Dover Publications, 2002.
2. Seychelles, F. and Amarouchene, Y. and Bessafi, M. and Kellay, H., Phys. Rev. Lett. **100**, 144501 (2008).
3. Priest, E.R., *Solar magneto-hydrodynamics*, Geophysics and astrophysics monographs, D. Reidel Pub. Co., 1984.
4. Tajima, T., *Computational plasma physics: with applications to fusion and astrophysics*, Frontiers in physics, Addison-Wesley, 1989.
5. T. Mullin and C. Blohm, Phys. of Fluids **13**, 136 (2001).
6. Andereck,C. David and Liu,S. S. and Swinney,Harry L., Journal of Fluid Mechanics **164**, 155 (1986).
7. Schrauf, G., Journal of Fluid Mechanics **166**, 287 (1986).
8. R. Benzi and S. Succi and Vergassola, Phys. Rep. **222**, 145 (1992).
9. S. Chen and G. Doolen, Annu. Rev. Fluid Mech. **30**, 329 (1998).
10. M. Mendoza and B. M. Boghosian and H. J. Herrmann and S. Succi, Phys. Rev. Lett. **105**, 014502 (2010).
11. Mendoza, M. and Herrmann, H. J. and Succi, S., Phys. Rev. Lett. **106**, 156601 (2011).
12. Hupp, D. and Mendoza, M. and Bouras, I. and Succi, S. and Herrmann, H. J., Phys. Rev. D **84**, 125015 (2011).
13. Halliday, I. and Hammond, L. A. and Care, C. M. and Good, K. and Stevens, A., Phys. Rev. E **64**, 011208 (2001).
14. X.D. Niu and C. Shu and Y.T. Chew, Int. J. Mod. Phys. C **14**, 785 (2002).
15. Klales, Anna and Cianci, Donato and Needell, Zachary and Meyer, David A. and Love, Peter J., Phys. Rev. E **82**, 046705 (2010).
16. Love, Peter J. and Cianci, Donato, Philosophical Transactions of the Royal Society A: Mathematical, Physical and Engineering Sciences **369**, 2362 (2011).
17. Grad, Harold, Communications on Pure and Applied Mathematics **2**, 325 (1949).
18. Martys, Nicos S. and Shan, Xiaowen and Chen, Hudong, Phys. Rev. E **58**, 6855 (1998).
19. Shan, Xiaowen and He, Xiaoyi, Phys. Rev. Lett. **80**, 65 (1998).
20. Chikatamarla, Shyam S. and Karlin, Iliya V., Phys. Rev. E **79**, 046701 (2009).

21. B. M. Boghosian and P. J. Love and P. V. Coveney and S. Succi and I. Karlin and J. Yepez, Phys. Rev. E Rapid Communications **68**, 025103 Part 2 (2003).
22. Karlin, Iliya V. and Gorban, Alexander N. and Succi, S. and Boffi, V., Phys. Rev. Lett. **81**, 6 (1998).
23. Mendoza, M. and Succi, S. and Herrmann, H.J., Sci. Rep. **3**, 3106 (2013).
24. Di Prima, R. and Swinney, Harry, volume, 45 of *Topics in Applied Physics*, Springer Berlin / Heidelberg, 1985.
25. F. Bartels, J. Fluid Mech. **119**, 1 (1982).
26. M. Wimmer, J. Fluid Mech. **78**, 317 (1976).
27. Richardson, L. F., Philosophical Transactions of the Royal Society of London. Series A, Containing Papers of a Mathematical or Physical Character **210**, 307 (1911).
28. Richardson, Lewis F. and Gaunt, J. Arthur, Philosophical Transactions of the Royal Society of London. Series A, Containing Papers of a Mathematical or Physical Character **226**, 299 (1927).